DOI：10. 11835/j. issn. 2096-6717. 2023. 131
开放科学(资源服务)标识码 OSID:

Formation mechanisms of a massive highway landslide in northern Pakistan

ASGHAR Aamir[1,2,3,4], *SU Lijun*[1,2,3], *ZHAO Bo*[1,2], *NIAZ Abrar*[5], *ULLAH Faheem*[1,2,3,4]

(1. Key Laboratory of Mountain Hazards and Earth Surface Process; Institute of Mountain Hazards and Environment, Chinese Academy of Sciences (CAS), Chengdu 610299, P. R. China; 2. University of Chinese Academy of Sciences, Beijing 100049, P. R. China; 3. China-Pakistan Joint Research Center on Earth Sciences, Islamabad, Pakistan; 4. The University of Poonch Rawalakot, Rawalakot 12350, Pakistan; 5.The University of Azad Jammu and Kashmir, Muzaffarabad 13100, Pakistan)

Abstract: Assessment of landslide hazards is important in highway engineering especially considering the landslide hazards along challenging roads; more research is needed to understand progressive strategies. Therefore, multidisciplinary and advanced methodologies were needed to assess the formation mechanisms and stability of complex landslides on the Muzaffarabad-Mansehra Highway in northern Pakistan. The main study objectives were to investigate slope failures, identify the triggering mechanism of layered rocks, image subsurface geometrical configurations, and assess slope stability factors using field operations, remote-sensing tools, geomorphological mapping, geophysical imaging, and kinematics analysis. The findings indicate that the foliated Hazara Formation, being buckled easily, is particularly susceptible to the geo-environmental conditions that triggered the landslide. Geophysical surveys revealed multiple layers of varying depth and thickness, highlighting the complexity of the landslide. Low resistivity zones (0.325-1 350 Ω·m) indicated the presence of un-onsolidated, water-saturated materials and highly sheared substances, whereas high resistivity zones (1 510-26 092 Ω·m) were associated with overburden, including alluvium, boulders, and dry slate fragments. Seismic refraction tomography indicated low P-wave velocities (400-1 800 m/s) within highly saturated overburdens, reworked blocks, and surficial weathering. The subsurface layers are interspersed with fragmented pieces of high-density rock and massive boulders, displaying P-wave velocities within the range of 3 000-5 000 m/s. Both tomographic methods revealed a fracture zone extending 30 m depth, which poses a significant risk of catastrophic occurrences. The sliding surface was found to be 25-30 meters depth at the crown and 45 meters depth in the main body. Kinematic analysis identified wedge failure as the primary failure mode along highway cuts. The findings of this study demonstrate the significance of employing integrated techniques to analyze the underlying mechanics of landslide hazards within the context of highway engineering. Furthermore, these integrated procedures are highly advantageous in efficiently eliminating the associated risks posed by such hazards.

Keywords: Lohar Gali landslide; foliated rocks; geomorphology; geophysical subsurface imaging; northern Pakistan

Received: 2023-07-04

Foundation items: National Natural Science Foundation of China (No. U22A20603); Strategic Priority Research Program of the Chinese Academy of Sciences (No. XDA20030301)

Author brief: ASGHAR Aamir, PhD candidate, main research interests: assessment of landslide hazards, E-mail: aamirasghar@imde.ac.cn.

SU Lijun (corresponding author), professor, doctoral supervisor, E-mail: sulijun1976@163.com.

巴基斯坦北部某大型公路滑坡的形成机理

ASGHAR Aamir[1,2,3,4],苏立君[1,2,3],赵波[1,2], NIAZ Abrar[5], ULLAH Faheem[1,2,3,4]

(1. 中国科学院 山地灾害与地表过程重点实验室;中国科学院、水利部成都山地灾害与环境研究所,成都 610299; 2. 中国科学院大学,北京 100049; 3. 中国-巴基斯坦地球科学联合研究中心,伊斯兰堡,巴基斯坦; 4. Poonch Rawalakot大学,Rawalakot 12350,巴基斯坦; 5. Azad Jammu and Kashmir大学,Muzaffarabad 13100,巴基斯坦)

摘 要:滑坡是山区公路安全运行的重要威胁,开展滑坡灾害评估尤为重要,尤其是深切峡谷区域的公路滑坡。以巴基斯坦北部Muzaffarabad-Mansehra公路沿线某大型滑坡为研究对象,采用野外调查、遥感分析、地貌解译、地球物理探勘和运动学分析等多种调查手段,进行滑坡的失稳特征、触发机理、地下结构特征和边坡稳定评估等研究,结果表明:滑坡发生在Hazara地层中,该地层以顺层斜坡为主,容易发生翘曲变形等破坏,属于滑坡易发地层。地球物理探勘表明:滑坡体内部存在多个不同深度和厚度的复杂结构,低电阻率区(0.325~1 350 Ω·m)以松散、饱水的堆积体为主,高电阻率区域(1 510~26 092 Ω·m)与覆盖层有关,包括冲积层、巨石和千板岩碎片等。地震反射层分析结果表明,在高度饱和的覆盖层、改造区块和表层风化层内,P波速度较低(400~1 800 m/s);而下垫层散布着高密度岩石碎片和大块巨石,P波速度为3 000~5 000 m/s。两种地球物理探勘结果均表明滑坡体内有一条延伸30 m深的破碎带,这是触发滑坡的重要因素。滑坡顶部的滑动面在深度25~30 m处,主体处的滑动面深度在45 m处。运动学分析表明:锲形体失稳是公路滑坡的主要破坏模式。研究结果表明,采用综合技术分析滑坡灾害的潜在机制可以有效减轻此类灾害带来的相关风险。

关键词:Lohar Gali滑坡;片状岩石;地貌学;地球物理成像;巴基斯坦北部

中图分类号:P642.22 **文献标志码**:A **文章编号**:2096-6717(2024)06-0051-19

1 Introduction

Landslides may substantially affect human populations, engineering structures, and the environment[1]. Massive slope failures have the potential to cause fatalities, physical damages, and relocation of individuals, destroying dwellings, transportation routes, bridges, and other essential facilities[2]. Northern Pakistan' s challenging topography and densely populated areas are prone to suffer severe infrastructure damages when landslides occur [3-4]. The steep inclines and unstable geological composition render it particularly vulnerable to landslides, which may be instigated by a variety of natural variables, such as intense precipitation, seismic events, and anthropogenic activities [5-6].

Although the vulnerability to landslides along challenging routes in northern Pakistan is recognized, additional research is necessary to improve the understanding of advanced techniques. The implementation of multidisciplinary methodologies based on ground-based field investigations, aerial photography gears, remote sensing tools, geomorphological mappings, lithological and structural failure modes, kinematic analysis, and comparative geophysical subsurface modeling needs to be addressed in the field of landslide research in this particular part of the world. Therefore, this study was designed to adopt a comprehensive combination of investigative techniques.

Landslides are often caused by geological features like steep slopes, weak rock or soil, weathering, drainage patterns, precipices, fault scarps, and escarpments with rock and water-soaked soil types on top of each other[7-8]. Notably, the existence of any of these geomorphological characteristics does not ensure the occurrence of a landslide but increases the probability of its occurrence[9]. These features should be evaluated together with other factors, such as weather, hydrological conditions, and historical records of landslides in the area[10]. Geophysical techniques are frequently employed in landslide investigations and engineering projects to discover soil and rock subsurface characteristics[11-12]. The techniques mentioned above have the potential to effectively

evaluate landslide risks and stability of slopes. However, their implementation can be financially burdensome[13-14]. Electrical resistivity tomography (ERT) and seismic refraction tomography (SRT) are non-invasive techniques that enable rapid surveying of vast regions and can be employed in remote or hard-to-reach locations. These techniques have been employed in numerous research activities to simulate landslides, and they are recognized as valuable tools for detecting possible landslide threats[15]. These techniques exhibit the ability to identify alterations in the subsurface lithological distributions, which may reveal the potential of a landslide.

These techniques can be employed to chart subsurface characteristics, including shear zones, fissures, and aquifers, that may contribute to landslides [16], and it has been supported by various studies [17-18]. There has been a growing trend toward utilizing geophysical surveys for landslide investigations in recent years owing to their ability to furnish significant insights into subsurface properties such as soil moisture content, the presence of fractures, and the depth of various layers. Furthermore, they enable the identification of geological structures and the characterization of the physical properties of soil and rock[19]. The position of the surface where sliding or slipping occurred was determined by scholars through the utilization of electrical resistivity tomography, seismic refraction tomography, and other geotechnical laboratory analyses, as reported by Pasierb et al. [20]. The accuracy of the interpretation is contingent upon various factors, including the quality of the data, the precision of the measurements, and the expertise of the interpreter, as noted by Kamiński et al. [21]. The disciplines of geology, geomorphology, and electrical resistivity tomography have been identified by Falae et al. [22] as interrelated fields that can be employed to investigate the surface and subsurface of the landslide. Collectively, these data sources can offer a more comprehensive depiction of exterior and interior features of a landslide. Here, we adopt the Lohar Gali landslide as a research object located on the Muzaffarabad-Mansehra Highway in northern Pakistan. The primary objective of this study is to offer an extensive understanding of landslides, particularly their occurrence along the highway. Our research aims to explain the formation process of slope failures, identify the mechanisms that initiate them, demarcate the vulnerable fractures, analyze the response of layered rocks, interpret the subsurface geometrical configurations, and assess the several factors that influence the stability of slopes within and beyond this particular region. Through the utilization of various approaches, this study aims to augment the capabilities of landslide research, enhance hazard assessment, and provide valuable contributions for the construction of effective solutions for mitigating landslides in the designated study area. The outcomes of this study should be useful for researchers and highway engineers when investigating and applying strategies to mitigate slope instability.

2 Study area

The Lohar Gali landslide is located in the northern region of Pakistan, precisely on the Muzaffarabad-Mansehra Highway, with coordinates ranging from 73°26′19″ to 73°26′40″ longitudes and 34°20′38″ to 34°20′51″ latitudes, approximately 3 km from the city center of Muzaffarabad, home to nearly one million inhabitants, and is linked to the Khyber Pakhtunkhwa (KP) province through this highway (Fig. 1(a)). The recent proposal to transform this highway into the Mansehra-Muzaffarabad-Mirpur-Mangla (MMMM) expressway has emerged as a decisive development, carrying profound implications from both strategic and socioeconomic perspectives. The region's challenging topography and climatic conditions pose persistent difficulties for travel and logistics activities, with frequent slope failures, rock falls, landslides, and other geological hazards [23]. The Lohar Gali landslide is located in the far west of the Muzaffarabad Fault and close to Jhelum Fault. Landslides in this area are well-known for their destructive impact on the local population and tourists (Fig. 1(c)). The Jhelum River flows along the toe of the landslide (Fig. 2(a)).

Tectonically, the Muzaffarabad region is located in the core of the Hazara-Kashmir Syntaxis (Fig. 1(b)), an active and complex tectonic element of the lesser and sub-Himalayan belt[25]. This belt is characterized by the presence of sedimentary rocks that have been deformed and uplifted by complex tectonic activity resulting from the convergence of the Indian and Eurasian plates[26-27].

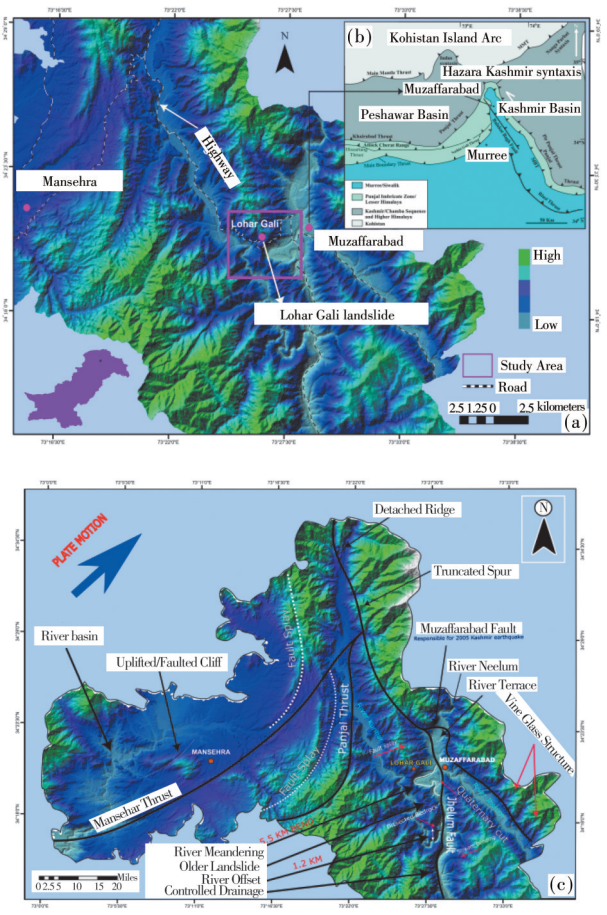

Notes: (a) Location map; (b) Hazara Kashmir Syntaxis revised from reference [24]; (c) Regional tectonic setting of the study area.

Fig. 1 Regional setting of the Lohar Gali landslide

The 7.6 Mw earthquake that struck Kashmir on October 8, 2005, accelerated the slope failure by reactivating many dormant landslides (Fig. 2(b)). A brief geomorphic analysis was conducted on the tectonic landform to comprehend the impact of regional faults on activating the Lohar Gali landslide, as depicted in Figs. 1(c) and 2(a). Typically, the structural information of a collisional mountain belt is conserved through the establishment and advancement of significant features at both micro and macro levels. These features systematically align and reflect the kinematics linked to the fault's history. Thus, it is necessary to thoroughly investigate these structural elements to understand the geomorphological phenomena connected to active faulting.

The Lohar Gali landslide is located on the hanging wall block of the Jhelum Fault (Fig. 2(a)). The trace of this oblique-slip fault traverses the eastern vicinity of the study area, where it has caused a displacement of the Kunhar River by 1.2 km on the surface (Fig. 2(a)). This displacement has resulted in the precise dissection of bedrock and other lithological units. The detailed analysis of remote sensing images shows that the Lohar Gali landslide is also intersected by a local fault splay with a north-south orientation, spanning 6 km (Fig. 1(c)).

The region exhibits diverse climatic and topographical features, with average temperatures ranging from 2 to 25 °C in winter and summer, respectively. Additionally, the area is significantly influenced by monsoon patterns that occur in June, July, and August, resulting in an average annual precipitation of 1 200 to 1 308 mm [29].

3 Methodology

3.1 Field survey and landform analysis

The study area was examined using geophysical techniques with UAV (Unmanned Aerial Vehicle) photographs and remote sensing images. A combination of fieldwork, satellite images, and a UAV (Phantom 4 Pro UAV) survey was used in the research methodology to investigate the geological and geomorphological distribution of the landslide[30]. The objective was to determine the underlying factors and intensity of slope instabilities, and acquire comprehensive data on landslide characteristics[31]. The data was utilized to delineate the regional and local geomorphic features and evaluate the geological composition and significant contributors of the landslide, as reported by Xiong et al. [7]. The methodology included geospatial analysis of the area and landslide topography, lithological characterization, quantification of slope inclination and orientation, and evaluation of vegetation cover by cartographic representation with maps and conceptual models (Figs. 1(c), 2(a), 4, 5, 6, 7, and 9(a)). In order to survey the upper and lower parts of the landslides, top-to-bottom carving erosional gullies were chosen for field traverses.

The joint data was collected from the outcrop exposed along the Lohar Gali landslide zone to perform kinematic analysis, enabling us to understand the nature of slope failure. Visual observations were used to determine the orientation of joints by Brunton Compass measurements and clinometer readings, while precise locations were taken by Trimble handset Global Positioning System (GPS). The present work employed DIPS (Data Interpretation using Projected Stereonets) to conduct kinematic analysis[32].

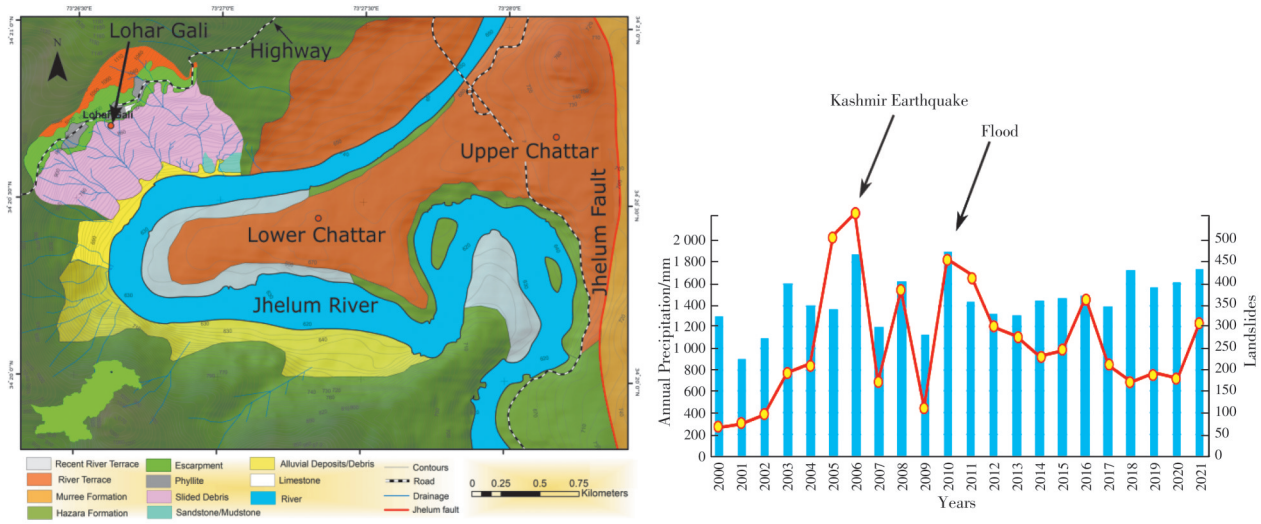

(a) Geological map

(b) Annual precipitation data and cumulative landslides, revised from reference [28]

Fig. 2　Geological setting and climate features of study area

The failure mode was subsequently evaluated in relation to the discontinuity's slope orientation and internal friction angle. Sardana et al. [33] stated that planar failure, toppling, and wedge failure are common on cut slopes.

The collected data were analyzed in the laboratory using software applications such as Pix4D, DroneDeploy, ArcGIS Desktop 10.8.1, and DIPS. Similarly, Wei et al. [34] conducted a field investigation to gather comprehensive data on the landslide's geological, geomorphological, and hydrological characteristics.

3.2　Geophysical investigations

3.2.1　Electrical Resistivity Tomography (ERT)

ERT is a method for figuring out the electrical resistivity distribution below the surfaces by measuring different types of resistance from electrodes that are arranged in a non-uniform geometric pattern [35-36]. This method uses penetrating waves to create sectional images of structures or objects, producing a tomogram as the resulting image for in-situ applications. As shown in Fig. 3(b), electrical resistivity tomography generates a tomogram to characterize the subsurface by evaluating the various resistive qualities of earth minerals through electrical resistivity[22-37]. This method has been successfully used for both geotechnical and geo-environmental applications [38].

A comprehensive field tour was organized to gather geophysical data on landslide geometrical configurations (Fig. 3(a)). There are many array configurations that can be used to collect data due to the different subsurface conditions; however, Wenner-Schlumberger electrode arrangements were chosen because they are commonly used and have been shown to be useful in examining subsurface variations that are both vertical and horizontal [39]. With the ABEM Terrameter SAS 4000 instrument from Sweden, the electrical resistivity tomography profiles were analyzed in two configurations, and enhancements were used to stimulate the subsurface for resistivity with depth in response to the induced electric field within the ground[40]. Electrodes (comprising both current and potential electrodes) were inserted into the ground to conduct the survey. Cables were then used to introduce current into the electrodes, while potential electrodes were utilized to measure the resulting potential difference. Several readings were carried out using these techniques along the selected lines in the study area. The spacing between electrodes was kept at 5 m in all electrical resistivity tomography profiles. Five profile lines were surveyed on the western section, while two profiles were carried out on the eastern section of the Lohar Gali landslide (Fig. 3(a)). The collected geo-electrical data was entered into the iteration software Res2DINV and Voxler to generate 2D geoelectric sections. The resistivity section delineated the horizontal and vertical extensions of the geoelectrical layers in the subsurface.

3.2.2 Seismic Refraction Tomography (SRT)

SRT is a methodology that utilizes travel time measurements of direct, refracted, and diffracted wave phases. The difference in velocity between waves is important for the method to work effectively. The behavior and physical properties of a material greatly influence how fast seismic waves can travel through it. Therefore, investigations into landslides that utilize this data to establish the failure surface and the physical properties of the landslide material have the potential to produce valuable outcomes. This has been demonstrated in previous studies[37-41]. By performing a tomographic inversion of the surface refraction data, it is possible to obtain a more comprehensive understanding of the subsurface. This method can reveal velocity variations in horizontal and vertical dimensions with improved resolution while also considering the complex internal structure of a landslide [12].

A two-dimensional (2D) seismic refraction tomography survey was conducted along different profiles at the research site, as depicted in Fig. 3. The instrumentation employed in the study comprised 24 vertically oriented geophones linked with Geometrics Geoide. The data was acquired by implementing a geophone spacing of 5 m along three intersecting lines. The profile lines span 200, 250, and 300 m at separate locations of the landslide body (Fig. 3(a)). To enhance the signal-to-noise (S/N) ratio, we conducted recordings at each geophone location and stacked each record at least five times. A cumulative sum of 48 common shot gathers (CSG) was procured throughout the investigation. The recording duration was 256 ms, with a sampling frequency of 0.125 ms. An 8-kilogram sledgehammer was utilized as a seismic source. The acquired data were processed and analyzed using software, namely Seisimager and Surfer.

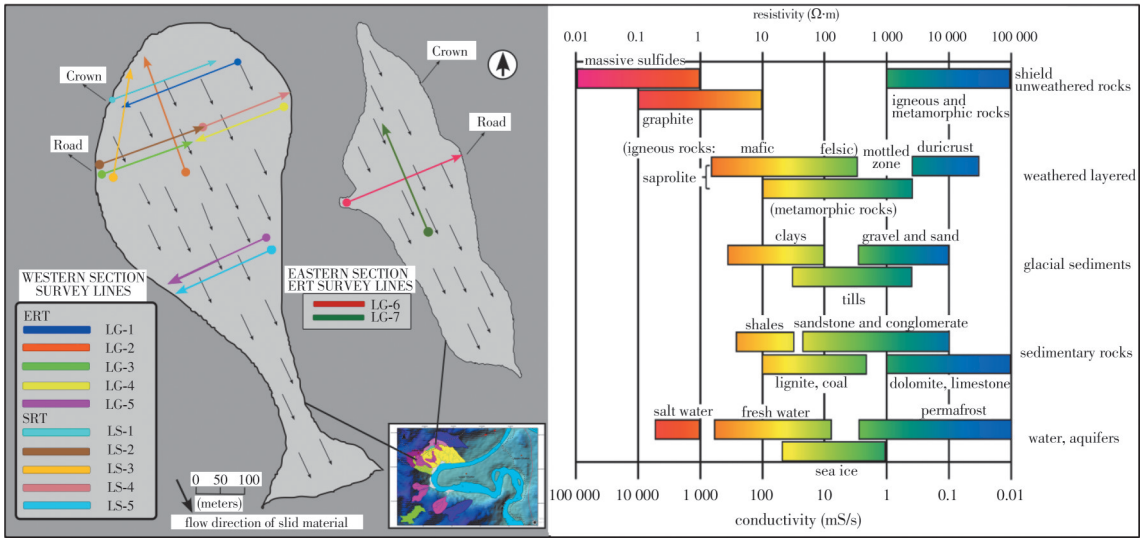

(a) ERT and SRT array lines for the geophysical investigation

(b) Resistivity chart for different types of rocks and soils, revised from reference [37]

Fig. 3 Geophysical investigation scheme at Lohar Gali landslide

4 Results and discussion

4.1 Basic description

The area affected by the Lohar Gali landslide (1.633 square kilometers) was partitioned into northern and southern zones, as illustrated in Fig. 4(a). These zones have been active since the 2005 earthquake (Fig. 4(b)). The northern zone is situated along the main highway, while the southern route is near the recently constructed powerhouse of the Patrind Hydropower Plant. For this comprehensive analysis we selected the northern zone due to its recurrent issues affecting the main highway route; this zone has a length of 2 km and a height ranging from 0.5 to 0.6 km (Fig. 4(a)). It is characterized by two active segments, one in the east and another one in the west (Figs. 5(a) and 6(a)). These active segments have heights ranging from 200 to 600 m with an inclination of 60° to 70°. Compared to the escarpment area, the angle of active segments beneath the main highway varies from 60° to 65°.

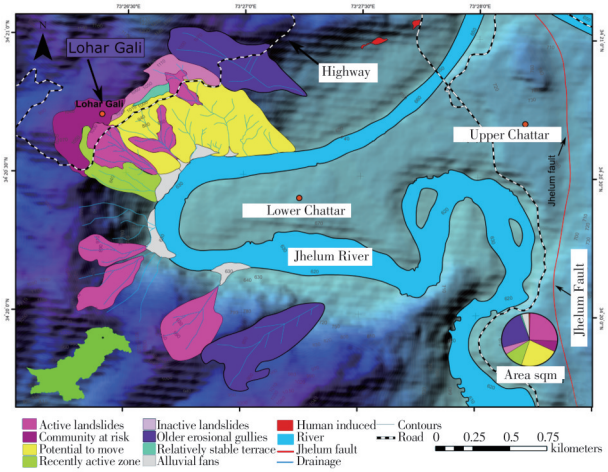

(a) Geomorphological distribution of the Lohar Gali landslide

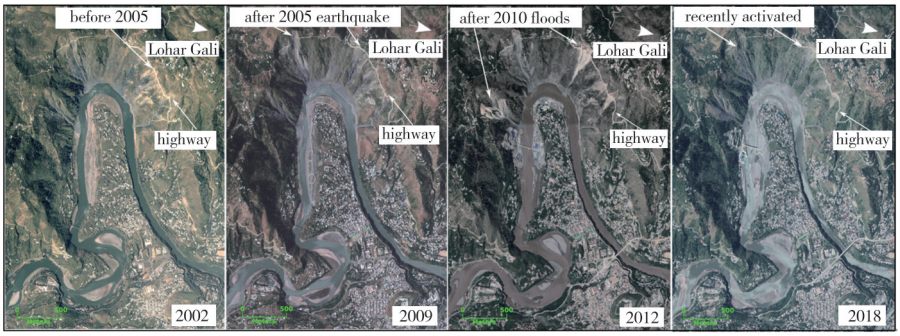

(b) Satellite images (Landsat-8) of the Lohar Gali landslide since 2002 showing different episodes of mass triggering along Muzaffarabad-Mansehra Highway

Fig. 4　Evolution process of the Lohar Gali landslide

According to the geological investigation conducted at Lohar Gali, it has been determined that the landslide area is primarily characterized by the Pre-Cambrian age Hazara Formation. This lithological formation is metamorphic and predominantly composed of shales, phyllites, and slates, with occasional occurrences of limestone (Fig. 2(a)). The lithologies described above have undergone weathering and deformation as a result of both geological and climatic factors. The shales and phyllites have a fine-grained texture, and their chromaticity displays a range from greyish green to blackish, with a subset turning to a dark greenish color during severe climatic conditions (Figs. 8 and 10). The uppermost part of the escarpment area, located adjacent to the main highway, comprises enormous overburdens and fragmented overhanging boulders, as illustrated in the longitudinal cross-section of the landslide (Fig. 9(b)). The escarpment is composed of colluvium and shales that dip downward at an inclination exceeding 60° (Fig. 8). The main body of the landslide comprises slid debris that exhibit angularity, fragmentation, and size variability. The slide area's flanks are distinguished by deformed and uncompacted shales and phyllites, mainly exhibiting fine to medium grain sizes and greenish-to-grey colors. The slid material comprises pebbles, gravels, and massive boulders that range from 1-150 cm in size and are sparsely distributed throughout the central part of the landslide.

The Jhelum River has been consistently washing out the toes of these active landslides as it flows in a meandering pattern. The tectonic activities of this area's compressional and transpressional regimes are significantly influenced by the nearby geological structures and a few small-scale splay faults. The segments affected by landslides display a dense yet inadequately managed drainage system carved into deformed shales, phyllites and slates.

4.2　Recently activated zones

4.2.1　Identifying activated zone

The western part of the landslide has been identified as having a high possibility of failures due to a newly activated fracture zone, which extends in a northeast-southwest direction and is demarcated by red

and yellow dotted lines in Fig. 5. The findings from the preliminary field investigations (conducted in March 2021 and October 2022) and the subsequent utilization of UAV aerial photography revealed that the fracture had undergone significant extension. Specifically, the fracture has extended to the crown of the active landslide measuring 400 m in length, surrounding an area of approximately 182 426 m^2 and has the potential to displace a volume of 7 297 040 m^3.

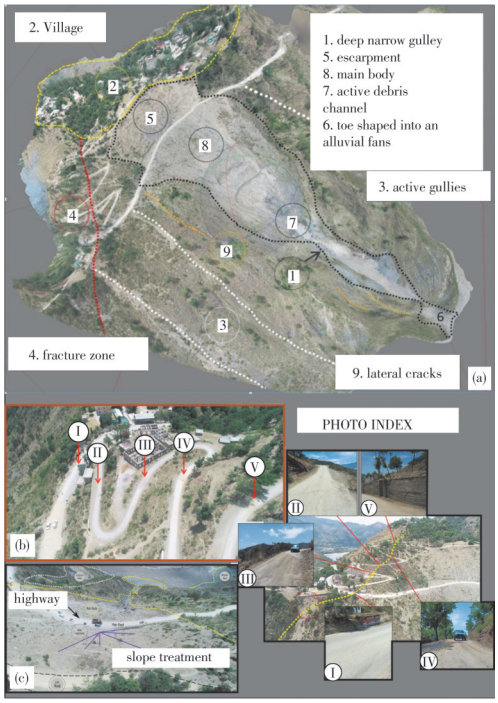

Notes: (a) Aerial view of the western section of the landslide; (b) The fracture zone with field photo index in which (I, II) shows subsidence up to 8 cm with minor lateral cracks, damaged retaining structure is shown in (V), while (III, IV) represents a oblique displacement of about 50 cm and 37 cm respectively; (c) is taken from the escarpment to display different landslide features.

Fig. 5 Deformation feature of the Lohar Gali landslide

Six active areas were found along this fracture by field investigations. III zone shows an oblique movement of 50 cm, while IV zone in Fig. 5(b) shows a vertical displacement of 37 cm. The projected crown of this fracture has been activated and marked with tilted trees. This has resulted in a rupture of 4 to 6 cm in the retaining wall structure, as depicted in Fig. 5(b). Meanwhile, the fractures at the remaining two locations (Figs. 5(a) and 5(b)) have not experienced any displacement but have undergone a subsidence of 6 to 8 cm. The appearance of wetness along these exposed fractures suggests the infiltration of precipitation, which may intensify the regions' instability and increase the landslide hazard (Figs. 6 and 8). Notably, the percolation of rainwater into the subsurface layers can result in increased instability and massive escalation of sliding material (Figs. 8, 9(a), and 10). The movement of this fracture zone has also caused the destabilization of a slope, leading to the subsidence of the constructed boundary wall of a government school and a residential building nearby.

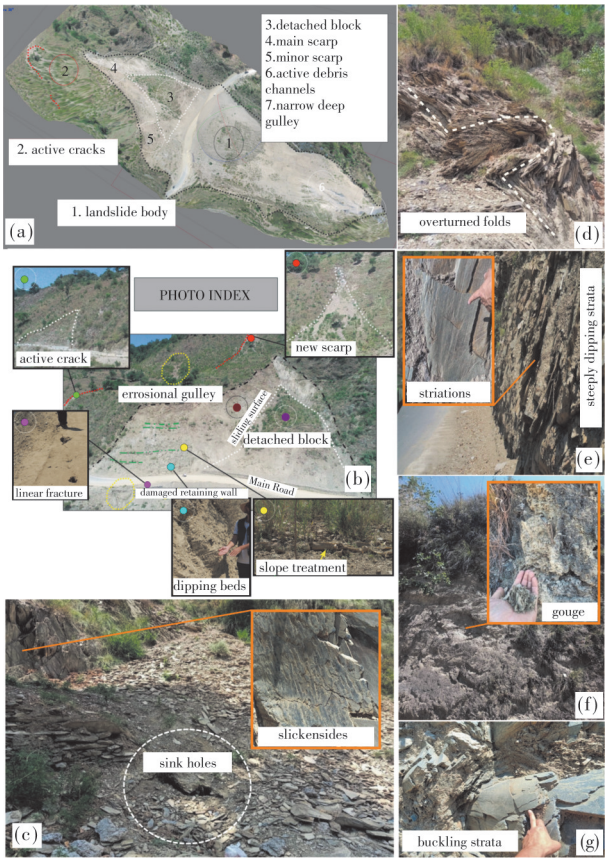

Notes: (a) Aerial view of the eastern section of Lohar Gali landslide; (b) Features associated with detached blocks; (c) Example of water seepages and slickensides; (d) Overturned northeast directions folding result of enormous stresses; (e) Steeply dipping strata shows striations of sliding over blocks,; (f) Highly imbricated shales metamorphosed into gouge material; (g) Bulging in slates due to unloading of overburden.

Fig. 6 Geological features of the Lohar Gali landslide

Besides this, the town of Lohar Gali comprises approximately 50 residential units situated on a scenic topography. The local people have a limited knowledge regarding the geological vulnerability of their surroundings (Figs. 4 and 5). The village is connected by a narrow roadway that traverses the escarpment of the western landslide segment. The drainage system on this link road is inadequate, resulting in the continuous refill of the tributaries. Insufficient sanitation infrastructure, including deficient sewerage systems and substandard septic tanks. After the 2005

earthquake, numerous houses were repaired or reconstructed. However, the ongoing subsidence has resulted in multiple new cracks in several houses. In light of the potential consequences of this fracture zone, we conducted a detailed survey utilizing geophysical techniques (ERT and SRT) to gain significant findings (Figs. 8 and 10).

4.2.2　Major contributors to landslide instability

Extensive landslides at Lohar Gali can be attributed to several factors, including geological, geo-environmental, and anthropogenic influences. This region experiences deformation due to tectonic forces, with notable geological features, such as the Jhelum Fault and Muzaffarabad Fault. These faults possess a seismic record and have been involved in notable earthquakes in the region [42]. This has led to the exposure of incompetent consolidated rocks of the Hazara Formation to tectonic deformation. The presence of steeply inclined, jointed, and faulted layers of shales, phyllites, and slates enhances the chance of slope failures due to the combined effects of gravity, overburden, topographic inclination, shear stresses, and climatic conditions. The significant accumulation of massive boulders and colluvium layers, particularly in the upper and central regions, has resulted in substantial slope loads, leading to slope failures (Figs. 8 and 10).

Besides this, the natural hydrological network and river cutting play a significant role in the genesis of drainage systems, parallel erosional gullies, and the deepening and expansion of the central and lower regions of landslides, particularly during the monsoon rainy seasons (Figs. 2(a), 4(b), 5(a) and 7).

Drainage System: The formation of the drainage system within a given region is subject to the influence of diverse geological factors, including tectonic activity, localized structures, and the lithological characteristics of rock formations [43]. Under insufficient drainage conditions, the rapid flow of water is obstructed, increasing pore pressure and decreasing soil strength. The decrease in strength can cause slope instability, which, in turn, can elevate the possibility of landslides [44]. The site mainly displays dendritic drainage patterns passing through unconsolidated loose materials. These patterns form a branching structure that emerges as streams flow downhill and sometimes converge into erosional gullies (Figs. 1(c), 2(a), 4(a), and 7). The Lohar Gali area features steeply inclined slopes that exhibit active lateral gullies and erosional surfaces. These features are intensified by inadequate surface drainage, leading to further erosion. In this case, the drainage system facilitates water penetration from the highway and accelerates the erosion process (Figs. 7 and 6(c)).

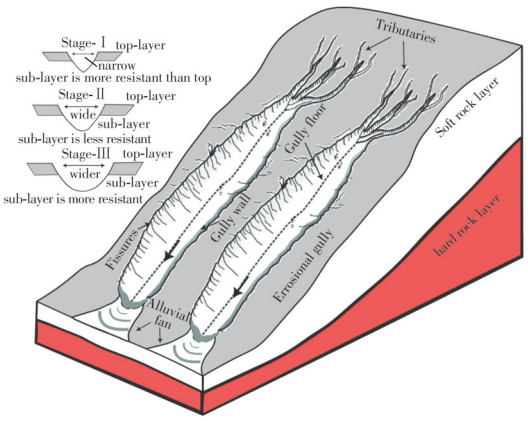

Fig. 7　Geomorphology of the erosional gully system

Besides natural drainage, the slopes above the Muzaffarabad-Mansehra Highway section are subjected to wastewater discharge from residential and agricultural areas, triggering landslides in the upper region. It is noteworthy that the research sites receive a constant influx of recharge from road drainage, community waste, and precipitation. The factors mentioned earlier worsen the drainage conditions, facilitating the emergence and advancement of landslides in the area.

Erosional Gullies: The morphology of landslides is significantly impacted by erosional gullies. Erosion channels are frequently formed through surface runoff linked with drainage systems and the consequent sediment, debris, and water transportation. This leads to the gradual carving of channels into the soil and soft layer of rock, as illustrated in the model (Fig. 7). The deepening and widening of these channels may compromise the stability of the slope, resulting in landslides [45]. The Lohar Gali landslide exhibited the presence of pre-existing erosional gullies within a distance of 400 m (southwest) to 600 m (northeast), covering about a total area of 394 595 m^2 (Fig. 4(a)). The northeast's erosional gulley system is positioned at 1 100 m above sea level (m. a. s. l) and discharges into a small urban settlement built

over the eroded debris at 830 m. a. s. l. The investigations found different geomorphic features, including gully floor/bed, gully walls, and gully fissures, and we identified three stages of erosion as shown in the model (Fig. 7). These active gullies display widths between 5 and 15 m and depths ranging from 3 to 7 m with a length from 75 to 300 m, as depicted in Fig. 5. The central region of the site lacks vegetation cover, in contrast to its periphery, owing to the uninterrupted downslope of material in the erosional and evolutionary processes of the area; ongoing activity contributes to the slope's failure (Fig. 3(a)). The area near active gullies displays the highest degree of severity and gradually expands towards the west, accompanied by a sizable fracture zone (Figs. 5, 8, and 10).

River Meandering: This process can lead to the undermining of slopes and substantial erosion, ultimately causing destabilization of the surrounding region [46].

The steeply inclined erosional gullies lead to the transportation of debris downstream, where it is subsequently deposited along the river's edges in the shape of alluvial fans (Figs. 4(a), 5(a), and 7). These deposits are highly susceptible to river currents, particularly in the flood season. The formation of alluvial fans in this region is attributed to the erosive action of rivers and their tributaries on the steep mountain slopes [47].

4.3 Subsurface geological structures

4.3.1 Interpretation and analysis of ERT data

In this research we employed electrical resistivity tomography to understand the subsurface characterization of the Lohar Gali landslide (Fig. 8 and Table 1). The survey exhibited a wide range of resistivity values, spanning from very low to very high, with a minimum of 0 and a maximum near 26 092 Ω·m (Fig. 8). These values were impacted by multiple factors, such as water-saturated fragments, water channels, deep dry fractures, deformed and undeformed strata of shales, phyllites, road-filling materials, and other dry materials such as boulders.

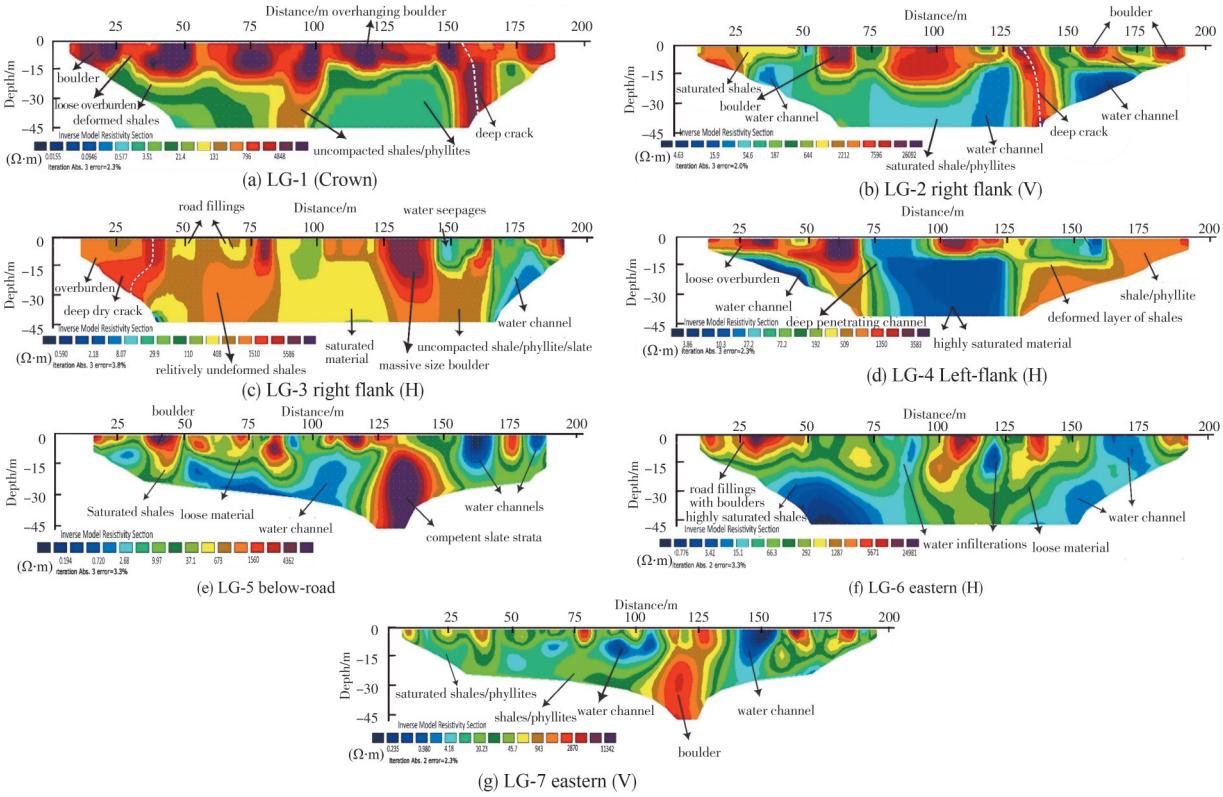

Fig. 8 Geoelectric sections of the electrical resistivity tomography survey at Lohar Gali Landslide; the locations of all geophysical lines are listed in Fig. 3(a)

Our findings indicate that the resistivity of fractured phyllites exhibits a range of values from 0 to 734 Ω·m. Lower resistivity values are observed in the presence of water, whereas higher resistivity values are associated with dry, intact rock subject to high confining pressure. This dryness is due to the closure of fractures and the consequent reduction of fluid flow in deeper areas (Table 1). The results indi-

Table 1　Overview of data acquisition and interpretation of electrical resistivity tomography results

ERT line/ array type	(length/ electrodes/ spacing)/m	max depth acquired/m	resistivity/(Ω·m)	lithological variations
LG-1 Wenner-Schlumberger	200/40/5	45	2. 07-21. 4	Saturated sheared slates and phyllites
			21. 5-131	Competent strata (slate)
			132-796	Loose overburden material
			797-4 848	Boulders and deep dry fracture
LG-2 Wenner-Schlumberger	200/40/5	45	0. 325-283	Deep water channel
			284-734	Saturated bedrock
			735-2 661	Loose overburden
			2 662-26 092	Deep dry fracture and boulders
LG-3 Wenner-Schlumberger	200/40/5	45	0. 598-29. 9	Water seepages and sheared loose material
			30-1 510	Loose overburden
			1 511-5 586	Competent strata and deep dry fractures
			5 587-11 974	Boulders
LG-4 Wenner-Schlumberger	200/40/5	45	1. 74-72. 2	Water seepages and saturated sheared loose fragments
			72. 3-401	Competent strata
			402-1 350	Dry overburden, Road fillings,
			1 351-3 583	Boulders
LG-5 Wenner-Schlumberger	200/40/5	45	0. 776-15. 1	Water-saturated fragments and water channels
			15. 2-292	Deep water flows through channels
			292-5 671	Competent strata of slates and phyllites
			5 672-24 981	Road Fillings and dry material with boulders.

cate that the entrance of water into the unconsolidated and fragmented rocks via sinkholes and fractures (Fig. 6(b) and 6(c)) has led to frequent landslides, particularly during rainy periods. The groundwater infiltration process reduces the shear strength of rock mass, thereby elevating the possibility of failure[48]; slates tend to fracture along planes of weakness, forming zones of instability in the subsurface. The presence of water can considerably diminish the shear strength of slopes, thereby making them more vulnerable to landslides. The horizontal survey line LG-3, which trends towards the south-east direction and runs parallel to the crown, has not revealed any evidence of water channels up to a depth of 45 m (Fig. 8). The survey lines LG-1 and LG-2 shows the existence of large boulders with significantly high resistivity values ranging from 3 929 to 26 092 Ω·m, as researchers found during their investigation of a landslide body [49]. These boulders are suspended at a steep angle of 70°, and their enormous size has resulted in additional load on the underlying loosely packed material. This pressure has resulted in an extensive deep dry fracture zone, ranging from 797 to 4 848 Ω·m, on the right side of the crown as demarcated by tomograms LG-2 and LG-3 (Fig. 8). Researchers [50] also reported deep fractures in their work. This phenomenon has consequently increased the chances of instability and movement (Figs. 6, 8, and 9).

The tomogram LG-2 has also identified three distinct water channels at a depth of 15 m, characterized by a resistivity range of 0. 325-283 Ω·m (Fig. 8). The results of the survey conducted on profiles LG-4 and LG-5 along the highway and the central portion indicate that main body exhibits water seepages, water channels, and highly saturated sheared material at relatively shallow depths [19]. Other researchers[16] also found seepages and sinkholes on the surface of landslides during resistivity investigations. Subsurface water typically follows channels that may become obstructed by sliding material, resulting in increased underground water pressure. This can further destabilize slopes and increase the chance of failures, allowing water to infiltrate deeper layers. Electrical resistivity tomography surveys on the lower portion (LG-5) have also confirmed the transformation of large rocks into the depletion region, as shown in Fig. 8; this transformation is recognized by a sparse distribution of boulders and shallow depth channels.

The electrical resistivity tomography models on the eastern section have revealed the presence of dry-

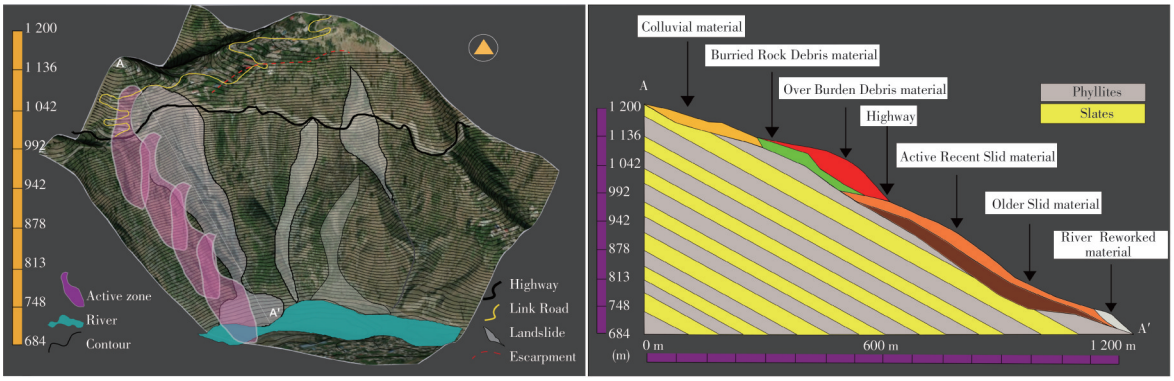

(a) Conceptual model for the vulnerable active block in the western section

(b) Schematic longitudinal cross-section of the Lohar Gali landslide

Fig.9 Location of active block and geological profile

filled road material and boulders (5 671-24 981 Ω·m) along with two shallow water channels within sheared loose material showing a resistivity range of 0.776-15.1 Ω·m as indicated in LG-6 (Fig. 8). On the other hand, in the array LG-7 we identified a region of medium resistivity values (10.23 Ω·m $<\rho<$ 2 870 Ω·m), which suggests the presence of deformed shales and phyllites (Fig. 8).

The subsurface lithology has been classified into three distinct layers through a comprehensive analysis of resistivity variations. The topmost stratum is composed of unconsolidated overburden materials, including alluvium, boulders, and dry road fills. The second layer comprises sheared and fractured shales and phyllites that slide over fragmented yet competent strata. The exact slip surface is more challenging to mark with ERT surveys; some scholars[51] revealed that the slip surface could be identified as the boundary between the upper unconsolidated deposits with a less resistive groundwater table and the lower hard, solid, and unweathered bedrock with high resistivity values. According to our investigations, the slip surface exhibits a depth range of 25 to 30 m in the crown region, while in the main body, the depth exceeds 45 m.

4.3.2 Interpretation and analysis of SRT results

Seismic refraction tomography was used to scan the Lohar Gali landslide's subsurface lithological distribution and geometry, as shown in Fig. 3(a). The results of this investigation demonstrate the landslides' depiction and the alignment of surficial fissures and fractures in greater depth. The velocity tomogram reveals a layered velocity pattern along the profiles, with an estimated mean depth of 30 m (Fig. 10). Beneath a stratum differentiated by a low P-wave velocity range of 400-1 800 m/s, there exists a layer with a relatively high P-wave velocity range of 2 000-3 000 m/s (Fig. 10). The geological formation comprises two layers of loose, unconsolidated materials, namely shales and phyllites, which have undergone saturation and deformation. These layers are interspersed with fragmented pieces of high-density rock and massive-sized boulders, exhibiting velocities within the 3 000-5 000 m/s range. The observed P-wave velocities ranging from 400 to 1 800 m/s indicate the highly saturated overburden, reworked blocks, and surficial weathering that is consistently present on the top of all the tomograms. The depth of this top layer ranges from 0 to 5 m and exhibits notable fractures in the LS-1, LS-2, and LS-3 models, respectively (Fig. 10). The second layer exhibits undulations and has a lateral extent of 200 m, with a thickness ranging from 5 to 7 m. This layer is characterized by the occurrence of unconsolidated saturated clay materials. Other researchers[41] found low velocities in a mixture of soil and weathered fragments in a landslide body in the Kundasang area of Sabah, Malaysia.

Seismic refraction tomographic data revealed three fractures within a horizontal range of 50-150 m. Notably, one of these fractures (Fracture-Ⅰ) is an extensive fracture that extends to a depth of 30 m (LS-1 and LS-2 in Fig. 10). The presence of fractures facilitates groundwater infiltration into the subsurface, thereby accelerating the flow of landslide material. Similarly, a team of researchers [52] marked a fracture zone of 25 m depth in the La Valette complex landslide of the South French Alps during seismic refrac-

tion investigations. The LS-1 model delineates a top surface layer, beneath which overhanging boulders exhibit P-wave velocities ranging from 4 000 to 5 000 m/s (Fig. 10). These boulders exert pressure on the underlying strata, and other contributing factors such as slope angle and gravity result in a rapid mass movement. Scholars [49] also identified massive boulders in the landslide body in the Xiaoshan district, China. The third layer comprises unconsolidated and deformed shales and phyllites, intermingled with large boulders of considerable magnitude that contain broken and fragmented pieces of bedrock. The P-wave velocity of the said layer ranges from 2 000 to 3 000 m/s, with an approximate total depth of 20 m (Fig. 10).

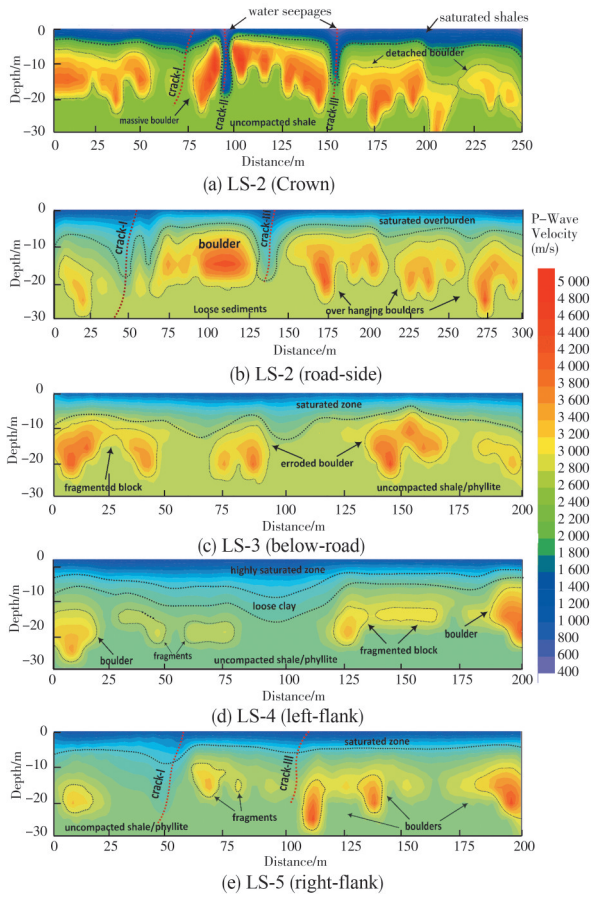

Fig. 10　SRT velocity sections conducted at Lohar Gali Landslide

The study compared the outcomes obtained from implementing electrical resistivity tomography and seismic refraction tomography, which are shown in Figs. 8 and 10, respectively. The tomograms of electrical resistivity (Ω·m) and P-wave velocity exhibit high similarity. The subsurface material of the landslides shows low resistivity values ranging from 0.325 to 1 350 Ω·m and low velocities ranging from 400 to 1 800 m/s. The low resistivity observed in this context can be attributed to highly saturated clays and loosely packed, overburdened materials. The detected rise in resistivity and P-wave velocity with depth can be attributed to comparably stiff and multiple lithological compositions. The high resistivities (1 510-26 092 Ω·m) and P-wave velocities (3 000 to 5 000 m/s) along the various profile lines indicate the occurrence of fragmented bedrock pieces and boulders (Figs. 8 and 10). Through detailed interpretation of resistivity and P-wave velocity variations, three distinct layers were identified in the subsurface. The investigation revealed that the slip surface displays a depth range of 25 to 30 m in the crown area, whereas in the main body, the depth surpasses 45 m. It is noteworthy that a fracture zone up to a depth of 30 m was identified by utilizing two distinct geophysical techniques (ERT and SRT). The findings of these subsurface techniques on the Lohar Gali landslide have furnished important information about the subsurface characteristics and revealed the landslide instigating elements.

4.4　Failure mechanism in layered rocks

Slope failure in stratified rock formations is the predominant geological hazard in the northwestern Himalayan region. The geomorphology of terrains is subject to continuous reshaping due to mounting stresses and weathering agents. However, it is essential to acknowledge that the exposed rock types also provide substantial resistance. The geological composition of the landslide outcrop area is characterized by foliated rocks, including shales, phyllite, schist, and slate, which exhibit a distinct layered structure. The layered rocks are bound by cleavage planes that are comparatively more susceptible to the continuing effects of precipitation, subsurface water channels, weathering, attrition, and gravity. Rainwater can infiltrate through fractures and permeate the vulnerable areas, leading to increased saturation and instability of the strata (Fig. 6(b)). When these relatively soft rocks are subjected to high weight, they can bend in the direction of the force, causing the underlying strata to be worn away and leaving smooth, polished surfaces with characteristic scratches and grooves (Fig. 6(a), 6(b), and 6(c)).

This phenomenon can lead to the movement of geological layers ranging from a few to several centimeters in magnitude, with the potential to extend as far as 250-300 m below the surface [53-54].

The consideration of various phases of structural deformation and their impact on foliations holds key importance in understanding failure mechanism in layered rocks (Fig. 11). The complex orientations of dip and strike in folded strata contributes to the complexity of failure kinematics and the observed displacements [55]. We prepared a modified model to explain the primary failure mechanism in layered rocks with considerable failure possibilities (Fig. 11). It was found that creeping, planar failure, wedge failure, and toppling depend upon the dipping angle and the orientation. At the same time, the compression and loading produce undulations, buckling, and fissures in the foliated rocks (Fig. 11). Researchers[56] have observed that metamorphic rocks tend to undergo creep along their dipping shear planes and penetrate to greater depths (Fig. 11(a) to 11(h)). However, in cases of anti-dipping, the strata

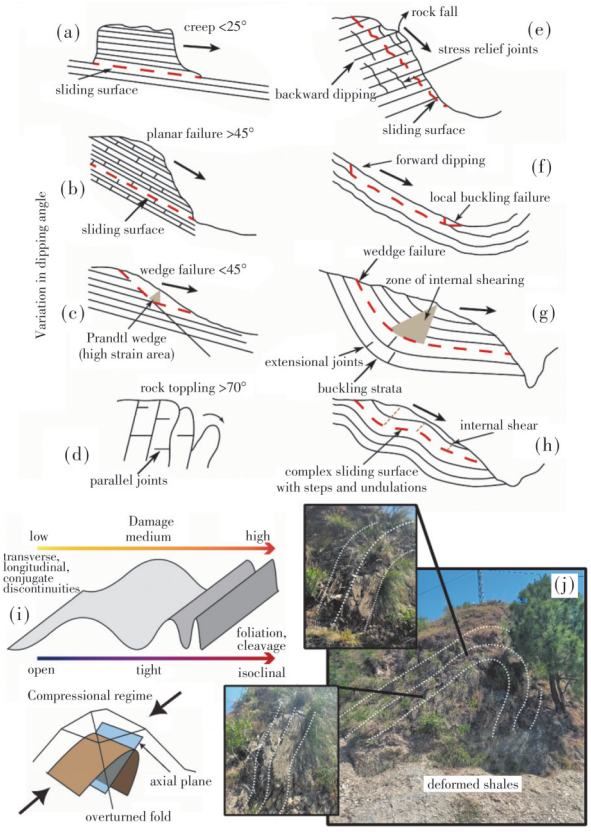

Notes: (a-h) Failure mechanism in layered rocks; (i and j) show the response of layered rocks in the Lohar Gali landslide area [55].

Fig. 11 Possible failure causes of the the Lohar Gali landslide

tend to topple (Fig. 11(d)). The deformation of foliated rocks is typically dependent upon the strength of the bindings of foliation. The foliated rocks continue to undergo deformation due to the force of gravity, resulting in buckling folds extending to the base of slopes. This deformation is evidenced by folded strata on the surface, as illustrated in Fig. 11(d). Similarly, the presence of overturned structures consisting of gouge and brecciated material in the layered rocks of the study area indicates that the landslide is structurally controlled and significantly squeezed by the regional compressions, which has compromised the rock strength and degree of weathering (Fig. 6(d) to 6(g)).

The weathering conditions experienced by metamorphic rocks have the potential to cause a reduction in the friction angle by a range of 8° to 10°. This can lead to a weakening of the rock's strength and an increase in the presence of clay minerals. As a result, the strength of slates may be reduced by as much as 30% to 50% [57]. Furthermore, the external loading of the boulders has the potential to cause the rupture of these rocks along their less robust cleavage plane, as documented in the literature[53-54]. The mechanism of slope deformation can also be achieved through the utilization of kinematic analysis. Therefore, a detailed analysis was performed to understand the failure mechanism of layered rocks.

4.5 Kinematic analysis along highway cuts

Joint orientation data was collected from 33 locations along the road cuts in the study area (Fig. 12). We merged data sets from different sites to understand potential failures at a broader level. The collected data consisted of coordinates (x, y), dip and dip direction, and lithological distribution, which are the necessary parameters for conducting kinematic analysis. The potential slope failure modes were investigated through kinematic analysis utilizing DIPS software [32-58]. The results have shown that wedge sliding (41.86 %) is the most prominent type of failure at varying slope angles of 60° to 70° with different ranges of friction angles (30° to 34°). The total of 33 poles has displayed a trend (120°) and plunge (28°) under the global best fit, a technique for figuring out how a mass is oriented and where it is placed relative to a fixed coordinate system (Fig. 12(b)).

Besides wedge failure, the probability of direct toppling was 36.3%, whereas the percentage of planar failure remained lower (Fig. 10(d)). Another study [33] found no planar failure along the highway cut from Kulikawn to Saikhamakawn of Aizawl, Mizoram, India.

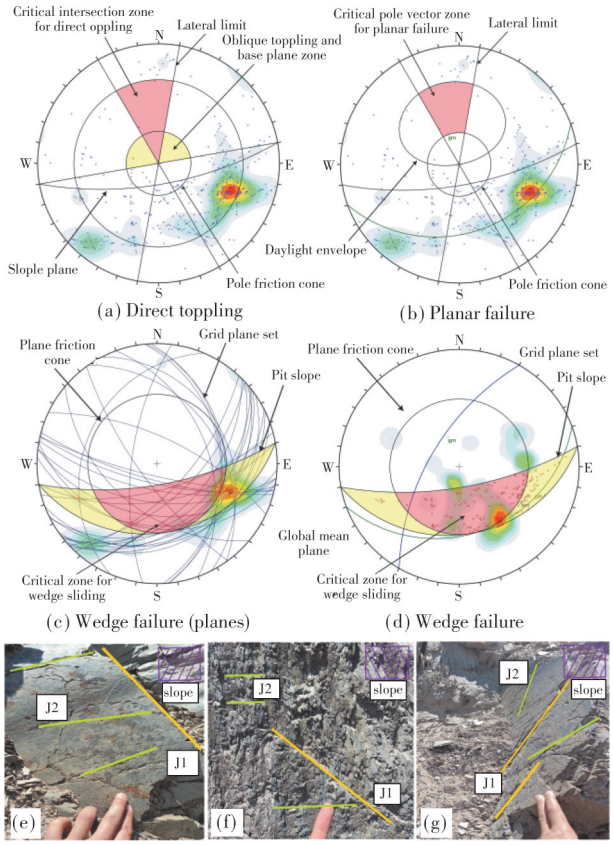

Notes: (a) Direct toppling; (b) Planar failure; (c) Wedge sliding with planes; (d) Wedge failure; (e, f and g) shows the joints orientation in the field.

Fig. 12　Kinematics analysis of the Lohar Gali landslide Kinematics analysis in DIPS

The ground data have shown that the exposed surficial Hazara Formation is mostly dragged, buckled, and overhung, justifying the dominant failure types found through the kinematic analysis. The mitigation of these failures is vital for the durability of highway engineering structure.

4.6　Highway engineering's significant outcomes

Road engineering plays a crucial role in ensuring the safety and dependability of transportation infrastructure [59]. The importance of slope instability lies in its potential to cause damage to highway users[60]. The Lohar Gali landslide has been the subject of recent research, highlighting the increasing importance of slope failures and their evaluation in highway engineering. This study focuses on conducting rigorous multidisciplinary scientific assessments to assist in efficient highway design, maintenance, environmental sustainability, and mitigation techniques. The research conducted on the Lohar Gali landslide has provided an understanding of the numerous factors contributing to slope instability in highway engineering, encompassing geological, geo-environmental, and human aspects. Some of these factors are regional stresses, lithological distribution (shales, phyllites, and slates), slope gradients (60° to 70°), intense precipitations, municipal wastewater, drainage characteristics, erosional gully formation, overburden deposition, rock fracturing, and river incision. Engineers must understand these variables to develop effective mitigation strategies for specific failure modes.

Our recent analyses show that the rocks in the research region feature gouged, brecciated, jointed, fractured, and buckled structures as a result of fault stresses (Figs. 1(c), 6(a)-6(g), and 11(a)-11(h)). Monsoon season precipitation makes these damaged rocks more unstable, causing widespread landslides (Fig. 2(b)). Slope failures are also increased by the lack of retaining and gabion structures, perforated pipework, channels, ditches, geotextiles, and geocomposite drains (Figs. 5(a) and 6(b)). Well-designed systems allow water to flow beneath roadways, protecting natural watercourses and reducing slope water pressure. Given these conditions, mitigation efforts should prioritize slope stabilization. The lack of drainage systems in the study area causes erosional gullies and slope failures (Fig. 7). Highway drainage systems must be maintained to reduce surface water runoff. This methodical strategy reduces slope instability and decline by limiting water accumulation. Untreated or insufficiently treated municipal wastewater into the ground weakens slope materials and landslides (Fig. 5(a)). Wastewater treatment systems on roadways reduce slope failure risk and improve slope stability. Poor excavations during highway clearance have caused slope instability by neglecting slope angle treatment, benching, and stabilization (Figs. 5(a) and 6(b)). Excavation techniques, especially for stratified road dipping rocks, needed improvement; their unprofessional handling led to unfortunate consequences (Figs. 6(b) and 11).

Geophysical engineering at Lohar Gali found overhanging boulders and road-filling cavities saturated by groundwater seepage into the weaker material, causing fracture extension (Figs. 6(c), 8, and 10). Removing massive boulders and water seepage control and redirection reduces loading, pore water pressure, erosion, and fractures, improving slope stability. Electrical resistivity and seismic refraction helped in classifying subsurface lithology, estimate slope stability, and identify slip surfaces. The landslide subsurface data modeling revealed a 30-meter-deep fracture zone (Figs. 8 and 10). Understanding these fracture zones is essential for efficient landslide management and risk mitigation. Geophysical methods improve slope science, aiding roadway engineering decision-making. Kinematic analysis reveals that wedge failure along highway cuts is the primary failure mechanism in the study region (Fig. 12). Engineers need to understand the specific way in which failures occur and find effective ways to prevent them to ensure the safety and stability of structures and roadway systems.

The study on the Lohar Gali landslide emphasizes the importance of multidisciplinary scientific evaluations to control and mitigate landslide hazards in road infrastructure. By integrating these approaches, highway engineers can potentially construct safer and more resilient transportation infrastructure for future generations.

5 Conclusions

The massive landslide in Lohar Gali has been triggered by various geological, geo-environmental, and human factors. Our research revealed that regional stresses, lithological composition, topography, precipitation, drainage system, erosional gullies, overburden, and river cutting significantly contributed to landslides in the study area. The area has a steep slope of 60° to 70°, with highly imbricated layers of shales, phyllites, and slates. These foliated rocks are more prone to severe climatic conditions. The natural drainage pattern has contributed to parallel gullies, which have deepened and enlarged the central section, particularly during monsoon seasons. The thick layers of colluvium and massive-sized boulders accumulated in the upper and central parts have created enormous loads on slopes, which are also responsible for slope failures.

The kinematic analysis concluded that the possibility of wedge failure is more than the toppling and planar failures along the highway cuts. The electrical resistivity and seismic refraction tomograms have shown similar results in characterizing subsurface lithological, hydrological, and geometrical configurations. The landslide material has low resistivity values of 0.325-1 350 Ω·m and low velocities of 400-1 800 m/s in highly saturated clays, loosely packed overburden material, and deformed shales. Near-surface and deep-water channels were also found during interpretations. The fragmented bedrock and massive-size boulders have high resistivities (1 510-26 092 Ω·m) and P-wave velocities (3 000 to 5 000 m/s). Variations in resistivity and P-wave velocity allowed to identify three layers in the subsurface lithology. It can be assumed that the slip surface is 25 to 30 m deep in the crown and 45 m deep in the accumulation zone.

The most significant finding of this research is the confirmation of a fracture zone that extends up to 30 m in depth and was previously identified during preliminary field investigations. With a vast volume of 7 297 040 m^3, this fracture zone is expected to block the Jhelum River, which would result in a catastrophic event. Anthropogenic activities, mainly the widening of the highway sections, have increased the slope angle, which exacerbates the failure potential. The findings of this study will provide valuable insights for researchers, highway engineers, and policymakers regarding slope failures and the effective management of landslide hazards.

References

[1] EMBERSON R, KIRSCHBAUM D, STANLEY T. New global characterisation of landslide exposure [J]. Natural Hazards and Earth System Sciences, 2020, 20(12): 3413-3424.

[2] WOUTER BOTZEN W J, DESCHENES O, SANDERS M. The economic impacts of natural disasters: A review of models and empirical studies [J]. Review of Environmental Economics and Policy, 2019, 13(2): 167-188.

[3] HUSSAIN M A, CHEN Z L, KALSOOM I, et al. Landslide susceptibility mapping using machine learning algorithm: A case study along Karakoram Highway

(KKH), Pakistan [J]. Journal of the Indian Society of Remote Sensing, 2022, 50(5): 849-866.

[4] KHAN H, SHAFIQUE M, KHAN M A, et al. Landslide susceptibility assessment using Frequency Ratio, a case study of northern Pakistan [J]. The Egyptian Journal of Remote Sensing and Space Science, 2019, 22(1): 11-24.

[5] SATI V P. Glacier bursts-triggered debris flow and flash flood in Rishi and Dhauli Ganga valleys: A study on its causes and consequences [J]. Natural Hazards Research, 2022, 2(1): 33-40.

[6] ULLAH K, WANG Y, FANG Z C, et al. Multi-hazard susceptibility mapping based on Convolutional Neural Networks [J]. Geoscience Frontiers, 2022, 13 (5): 101425.

[7] XIONG L Y, LI S J, TANG G A, et al. Geomorphometry and terrain analysis: Data, methods, platforms and applications [J]. Earth-Science Reviews, 2022, 233: 104191.

[8] ZHAO B, WANG Y S, LI W L, et al. Evaluation of factors controlling the spatial and size distributions of landslides, 2021 Nippes earthquake, Haiti [J]. Geomorphology, 2022, 415: 108419.

[9] CHEN B, LI Z H, ZHANG C L, et al. Wide area detection and distribution characteristics of landslides along Sichuan expressways [J]. Remote Sensing, 2022, 14(14): 3431.

[10] CHETTRI N, TEMPA K, GURUNG L, et al. Association of climate change to landslide vulnerability and occurrences in Bhutan [M]//SARKAR R, SHAW R, PRADHAN B. Impact of climate change, land use and land cover, and socio-economic dynamics on landslides. Singapore: Springer, 2022: 3-37.

[11] SU L J, XU X Q, GENG X Y, et al. An integrated geophysical approach for investigating hydro-geological characteristics of a debris landslide in the Wenchuan earthquake area [J]. Engineering Geology, 2017, 219: 52-63.

[12] ULLAH F, SU L J, ALAM M, et al. Landslide stability investigation and subsurface deformation mapping by optimizing low-frequency GPR: A mega rainfall susceptible landslide case study (Gilgit Baltistan, Pakistan) [J]. Bulletin of Engineering Geology and the Environment, 2022, 81(9): 373.

[13] DERIE B M. Integration of geophysical methods for groundwater exploration in hard rock areas: Application to Alla Valley, Eritrea, NE Africa [D]. Loughborough: Loughborough University, 2011.

[14] POPOOLA O I, ADENUGA O A. Determination of leachate curtailment capacity of selected dumpsites in Ogun State southwestern Nigeria using integrated geophysical methods [J]. Scientific African, 2019, 6: e00208.

[15] LAPENNA V, PERRONE A. Time-lapse electrical resistivity tomography (TL-ERT) for landslide monitoring: Recent advances and future directions [J]. Applied Sciences, 2022, 12(3): 1425.

[16] FALAE P O, DASH R K, KANUNGO D P, et al. Interpretation on water seepage and degree of weathering in a landslide based on pre- and post-monsoon electrical resistivity tomography [J]. Near Surface Geophysics, 2021, 19(3): 315-333.

[17] ARAUJO S, GUZMÁN O, GUAMÁN A, et al. Seismic refraction tomography in San Luis, headward Coca River erosion zone [J]. Journal of Applied Geophysics, 2023, 212: 104981.

[18] WAGNER F M, UHLEMANN S. An overview of multimethod imaging approaches in environmental geophysics [J]. Advances in Geophysics, 2021, 62: 1-72.

[19] SIGDEL A, ADHIKARI R K. Application of Electrical Resistivity Tomography (ERT) survey for investigation of the landslide: A case study from Taprang landslide, Kaski district, west-central Nepal [J]. Journal of Nepal Geological Society, 2020, 60: 103-115.

[20] PASIERB B, GRODECKI M, GWÓŹDŹ R. Geophysical and geotechnical approach to a landslide stability assessment: A case study [J]. Acta Geophysica, 2019, 67 (6): 1823-1834.

[21] KAMIŃSKI M, ZIENTARA P, KRAWCZYK M. Electrical resistivity tomography and digital aerial photogrammetry in the research of the "Bachledzki Hill" active landslide - in Podhale (Poland) [J]. Engineering Geology, 2021, 285: 106004.

[22] FALAE P O, KANUNGO D P, CHAUHAN P K S, et al. Electrical resistivity tomography (ERT) based subsurface characterisation of Pakhi Landslide, Garhwal Himalayas, India [J]. Environmental Earth Sciences, 2019, 78(14): 1-18.

[23] ASGHAR A, SU L J, ZHAO B, et al. Integrating predictive modeling techniques with geospatial data for landslide susceptibility assessment in northern Pakistan [J]. Journal of Mountain Science, 2023, 20(9): 2603-2627.

[24] ALI A, FAISAL S, REHMAN K, et al. Tectonic imprints of the Hazara Kashmir Syntaxis on the Northwest Himalayan fold and thrust belt, North Pakistan [J]. Arabian Journal of Geosciences, 2015, 8(11): 9857-9876.

[25] QASIM M, TANOLI J I, AHMAD L, et al. First U-Pb detrital zircon ages from Kamlial formation (Kashmir, Pakistan): Tectonic implications for Himalayan Exhumation[J]. Minerals, 2022, 12(3): 298.

[26] FU R S, HUANG J H, XU Y M, et al. Numerical simulation of the collision between Indian and Eurasian

Plates and the deformations of the present Chinese continent [J]. Acta Seismologica Sinica, 2000, 13(1): 1-7.

[27] SAKAWAT HOSSAIN M, SHARIF HOSSAIN KHAN M, ABDULLAH R, et al. Tectonic development of the Bengal Basin in relation to fold-thrust belt to the east and to the north [M]//BISWAL T, RAY S, GRASEMANN B. Structural geometry of mobile belts of the Indian subcontinent. Cham: Springer, 2020: 91-109.

[28] KHAN M A, BASHARAT M, RIAZ M T, et al. An integrated geotechnical and geophysical investigation of a catastrophic landslide in the Northeast Himalayas of Pakistan [J]. Geological Journal, 2021, 56(9): 4760-4778.

[29] PMD. Pakistan Meteorological Department [EB/OL]. https://www.pmd.gov.pk/en/.

[30] VALKANIOTIS S, PAPATHANASSIOU G, GANAS A. Mapping an earthquake-induced landslide based on UAV imagery; case study of the 2015 Okeanos landslide, Lefkada, Greece [J]. Engineering Geology, 2018, 245: 141-152.

[31] HUANG F M, CHEN L X, YIN K L, et al. Object-oriented change detection and damage assessment using high-resolution remote sensing images, Tangjiao Landslide, Three Gorges Reservoir, China [J]. Environmental Earth Sciences, 2018, 77(5): 183.

[32] ROCSCIENCE. DIPS version 6.0, interactive analysis of orientation based geological data [EB/OL]. [2023-03-12]. https://www.rocscience.com/software/dips.

[33] SARDANA S, VERMA A K, VERMA R, et al. Rock slope stability along road cut of Kulikawn to Saikhamakawn of Aizawl, Mizoram, India [J]. Natural Hazards, 2019, 99(2): 753-767.

[34] WEI X S, FAN W, CHAI X Q, et al. Field and numerical investigations on triggering mechanism in typical rainfall-induced shallow landslides: A case study in the Ren River Catchment, China [J]. Natural Hazards, 2020, 103(2): 2145-2170.

[35] DAILY W, RAMIREZ A, BINLEY A, et al. Electrical resistance tomography [J]. The Leading Edge, 2004, 23(5): 438-442.

[36] JIANG L C, TIAN G, WANG B B, et al. Application of three-dimensional electrical resistivity tomography in urban zones by arbitrary electrode distribution survey design [J]. Journal of Applied Geophysics, 2021, 194: 104460.

[37] PALACKY G J. Resistivity characteristics of geologic targets [M]//NABIGHIAN M N. Electromagnetic methods in applied geophysics. Houston: Society of Exploration Geophysicists, 1988: 52-129.

[38] DAFALLA M, ALFOUZAN F. Electrical resistivity tomography of a gypsiferous subsurface soil: Geotechnical detection of a geoenvironmental phenomenon [J]. Journal of King Saud University - Science, 2023, 35(4): 102595.

[39] TONGKELES P V, SURYANTINI, PRATAMA A B. The application of electrical resistivity tomography using wenner-schlumberger arrays configuration to identify the geological structure in kancah warm spring, West Java Indonesia [J]. IOP Conference Series: Earth and Environmental Science, 2022, 1047(1): 012015.

[40] NIAZ A, KHAN M R, IJAZ U, et al. Determination of groundwater potential by using geoelectrical method and petrographic analysis in Rawalakot and adjacent areas of Azad Kashmir, sub-Himalayas, Pakistan [J]. Arabian Journal of Geosciences, 2018, 11(16): 468.

[41] ABIDIN M Z, SAAD R, AHMAD F, et al. Seismic refraction investigation on near surface landslides at the Kundasang area in Sabah, Malaysia [J]. Procedia Engineering, 2012, 50: 516-531.

[42] BASHARAT M, RIAZ M T, JAN M Q, et al. A review of landslides related to the 2005 Kashmir Earthquake: Implication and future challenges [J]. Natural Hazards, 2021, 108(1): 1-30.

[43] RÓŻYCKA M, JANCEWICZ K, MIGOŃ P, et al. Tectonic versus rock-controlled mountain fronts- Geomorphometric and geostatistical approach (Sowie Mts., Central Europe) [J]. Geomorphology, 2021, 373: 107485.

[44] KUSÁK M. Application of fractal and multifractal analysis on Blue Nile drainage patterns in the morphostructural analysis of the Ethiopian Highlands, Ethiopia [J]. Progress in Physical Geography: Earth and Environment, 2022, 46(3): 357-370.

[45] REED M, KITE S. Peripheral gully and landslide erosion on an extreme anthropogenic landscape produced by mountaintop removal coal mining [J]. Earth Surface Processes and Landforms, 2020, 45(9): 2078-2090.

[46] LO P C, LO W, CHIU Y C, et al. Movement characteristics of a creeping slope influenced by river erosion and aggradation: Study of Xinwulü River in southeastern Taiwan [J]. Engineering Geology, 2021, 295: 106443.

[47] BIBI M, WAGREICH M, IQBAL S, et al. Regional sediment sources versus the Indus River system: The Plio-Pleistocene of the Peshawar Basin (NW-Pakistan) [J]. Sedimentary Geology, 2019, 389: 26-41.

[48] SINGH P K, SINGH K K, SINGH T N. Slope failure in stratified rocks: A case from NE Himalaya, India [J]. Landslides, 2017, 14(4): 1319-1331.

[49] IMANI P, TIAN G, HADILOO S, et al. Application of combined electrical resistivity tomography (ERT) and

seismic refraction tomography (SRT) methods to investigate Xiaoshan District landslide site: Hangzhou, China [J]. Journal of Applied Geophysics, 2021, 184: 104236.

[50] NAGAIAH E, SONKAMBLE S, CHANDRA S. Electrical geophysical techniques pin-pointing the bedrock fractures for groundwater exploration in granitic hard rocks of Southern India [J]. Journal of Applied Geophysics, 2022, 199: 104610.

[51] GAN J J, ZHANG Y X, LIU X. An application of the high-density electrical resistivity method for detecting slide zones in deep-seated landslides in limestone areas [J]. Journal of Applied Geophysics, 2020, 177: 104013.

[52] SAMYN K, TRAVELLETTI J, BITRI A, et al. Characterization of a landslide geometry using 3D seismic refraction traveltime tomography: The La Valette landslide case history [J]. Journal of Applied Geophysics, 2012, 86: 120-132.

[53] BLIKRA L H. The Åknes rockslide, Norway [M]// CLAGUE J J, Stead D. Landslides: Types, mechanisms and modeling. Cambridge: Cambridge University Press, 2013.

[54] STROM A. Mechanism of stratification and abnormal crushing of rockslide deposits [C]//Proc. 7th International IAEG Congress. Balkema Rotterdam, 1994.

[55] STEAD D, WOLTER A. A critical review of rock slope failure mechanisms: The importance of structural geology [J]. Journal of Structural Geology, 2015, 74: 1-23.

[56] HUANG D, MA H, HUANG R Q, et al. Deep-seated toppling deformations at the dam site of the Miaowei Hydropower Station, Southwest China [J]. Engineering Geology, 2022, 303: 106654.

[57] CALCATERRA D, GILI J A, IOVINELLI R. Shallow landslides in deeply weathered slates of the Sierra de Collcerola (Catalonian Coastal Range, Spain) [J]. Engineering Geology, 1998, 50(3/4): 283-298.

[58] JAISWAL A, VERMA A K, SINGH T N. Evaluation of slope stability through rock mass classification and kinematic analysis of some major slopes along NH-1A from Ramban to Banihal, North Western Himalayas [J]. Journal of Rock Mechanics and Geotechnical Engineering, 2023

[59] SARDANA S, VERMA A K, SINGH A, et al. Comparative analysis of rockmass characterization techniques for the stability prediction of road cut slopes along NH-44A, Mizoram, India [J]. Bulletin of Engineering Geology and the Environment, 2019, 78(8): 5977-5989.

[60] AECOM A. Spon's civil engineering and highway works price book 2020 [M]. Florida: CRC Press, 2019.

(编辑　胡英奎)